



Article

Facile Electrochemical Sensor for Nanomolar Rutin Detection Based on Magnetite Nanoparticles and Reduced Graphene Oxide Decorated Electrode

Quanguo He ^{1,2,3,†}, Yiyong Wu ^{1,2,†}, Yaling Tian ^{1,2,†}, Guangli Li ¹, Jun Liu ¹, Peihong Deng ^{2,3,*} and Dongchu Chen ^{3,*}

¹ School of Life Sciences and Chemistry, Hunan University of Technology, Zhuzhou 412007, China; hequanguo@126.com (Q.H.); wyy5082010@163.com (Y.W.); tianyaling0212@163.com (Y.T.); guangli010@hut.edu.cn (G.L.); liu.jun.1015@163.com (J.L.)

² Hunan Provincial Key Laboratory of Functional Metal-Organic Compounds; Key Laboratory of functional Organometallic Materials of Hunan Provincial Universities; Department of Chemistry and Material Science, Hengyang Normal University, Hengyang 421008, China

³ School of Materials Science and Energy Engineering, Foshan University, Foshan 528000, China

* Correspondence: dph1975@163.com (P.D.); chendc@fosu.edu.cn (D.C.); Tel./Fax: +86-731-2218-3383 (P.D. & D.C.)

† These authors contributed equally to this work.

Received: 24 December 2018; Accepted: 14 January 2019; Published: 18 January 2019



Abstract: A new electrochemical sensor for nanomolar rutin detection based on amine-functionalized Fe₃O₄ nanoparticles and electrochemically reduced graphene oxide nanocomposite modified glassy carbon electrode (NH₂-Fe₃O₄ NPs-ErGO/GCE) was fabricated through a simple method, and the X-ray diffraction (XRD), Fourier transform infrared spectroscopy (FTIR), scanning electron microscope (SEM), transmission electron microscope (TEM), vibrating sample magnetometer (VSM) and electrochemical technique were used to characterize the modified electrode. The electrochemical behavior of rutin on the Fe₃O₄ NPs-ErGO/GCE was studied in detail. The electrochemical response of rutin at this modified electrode was remarkably higher than that of the bare GCE or other modified GCE (GO/GCE, Fe₃O₄ NPs-GO/GCE, and ErGO/GCE). Under the optimum determination conditions, Fe₃O₄ NPs-ErGO/GCE provided rutin with a broader detection range of 6.0 nM–0.1 μM; 0.1–8.0 μM and 8.0–80 μM, a minimum detectable concentration of 4.0 nM was obtained after 210 s accumulation. This novel method was applied in determination of rutin in pharmaceutical tablets and urine samples with satisfactory results.

Keywords: rutin; amine-functionalized Fe₃O₄ nanoparticles; electrochemically reduced graphene oxide; nanomolar electroanalysis

1. Introduction

Flavonoids are a kind of natural product widely existing in plants. They have antioxidant and anti-free radical effects and can be used in the treatment of cardiovascular and cerebrovascular diseases, tumors, inflammation and so on. Rutin (3',4',5,7-tetrahydroxyflavone-3-d-rutinoside), also known as vitamin P, is a common flavonoid glycoside widely present in many plants, especially in buckwheat plants [1]. Modern pharmacological studies have found that rutin not only regulates the permeability and fragility of the capillary wall, prevents vascular rupture and hemostasis, but also has the effects of anti-bacterial, anti-inflammatory, analgesic, anti-radiation, anti-oxidation, anti-myocardial hypoxia, reducing serum cholesterol, diuresis, spasmolysis and inhibiting platelet aggregation [2,3]. Therefore, it is of great significance to develop simple, reliable and sensitive methods for rutin analysis.

So far, numerous analysis methods, such as high performance liquid chromatography [4,5], chemiluminescence [6,7], capillary electrophoresis [8], spectrophotometry [9], flow injection analysis [10] and electrochemistry [11] have been reported for the determination of rutin. Among these methods, some involve expensive equipment, a time-consuming process, the use of toxic organic reagents or poor sensitivity. Electrochemical methods have the virtues of low-cost apparatus, high sensitivity, wide linear range and simplicity. Due to the electroactivity of rutin, various electrodes have been modified and explored for the detection of rutin [12–20], and their typical analytical figures of merit for rutin analysis are compared and summarized in Table 1. In order to amplify the response signal fundamentally and improve the detection sensitivity practically, it is still important and necessary to develop new electrochemical sensors for rutin detection at the nanomolar level.

Table 1. Electrochemical response data of rutin (10 μ M) at different decorated electrodes.

| Working Electrodes | $i_{pa}/\mu A$ | $i_{pc}/\mu A$ | E_{pa}/V | E_{pc}/V | i_{pa}/i_{pc} | ΔE_p |
|---|----------------|----------------|------------|------------|-----------------|--------------|
| ^a GCE | 1.431 | 1.093 | 0.674 | 0.653 | 1.309 | 0.021 |
| ^b GO/GCE | 0.5843 | 0.309 | 0.676 | 0.651 | 1.890 | 0.025 |
| ^c NH ₂ -Fe ₃ O ₄ NPs-GO/GCE | 2.396 | 1.929 | 0.678 | 0.657 | 1.242 | 0.021 |
| ^d ErGO/GCE | 14.35 | 13.58 | 0.678 | 0.661 | 1.057 | 0.017 |
| ^e NH ₂ -Fe ₃ O ₄ NPs-ErGO/GCE | 21.16 | 17.00 | 0.663 | 0.648 | 1.245 | 0.015 |

^a glassy carbon electrode; ^b graphene oxide modified glassy carbon electrode; ^c amine-functionalized Fe₃O₄ nanoparticles modified glassy carbon electrode; ^d electrochemically reduced graphene oxide modified glassy carbon electrode; ^e amine-functionalized Fe₃O₄ nanoparticles decorated electrochemically reduced graphene oxide modified glassy carbon electrode.

Since graphene (GR) was first reported in 2004, this two-dimensional carbon nanomaterial has attracted tremendous attention due to its excellent properties such as high surface area, fast electron transportation, excellent mechanical strength, high thermal conductivity and high mobility of charge carriers [21]. In recent years, great progress has been made in GR based nanocomposites by utilizing the synergistic effect of the components used. GR has been combined with different material entities such as metal, metal oxide, biomolecules and polymers, and the nanocomposites can provide their individual advantages of each component and demonstrate an improved performance [22–30]. Fe₃O₄ nanoparticles (Fe₃O₄ NPs) are widely used in the biomedical field because of their good biocompatibility, low cost, easy preparation, large surface area and distinct catalytic activity [31–33]. However, Fe₃O₄ NPs exhibit poor performance on electrical conductivity and are inclined to agglomerate, which hampers their application in electrochemical sensors [34]. The fabrication and application of GR and Fe₃O₄ NPs composite has been explored recently. For example, Zhang et al. fabricated a Nafion covered core-shell structured Fe₃O₄@graphene nanospheres modified glassy carbon electrode (GCE) and used it for selective detection of dopamine [35]. Yin et al. prepared a nanosized graphene, chitosan and Fe₃O₄ composite as electrode material which exhibited an excellent electrocatalytic and adsorptive activity towards the oxidation of guanosine [36]. Teymourian et al. synthesized GR/Fe₃O₄ nanohybrids via a facile one-step chemical reaction strategy, where the reduction of graphene oxide (GO) and the in-situ generation of Fe₃O₄ nanoparticles occurred simultaneously, which showed good electrochemical behaviors toward the oxidation of NADH [37]. Sun et al. prepared various shapes (sphere, rod and band) Fe₃O₄ decorated reduced graphene oxide (rGO) via one-step co-precipitation route in solution. It was proved that the shapes of Fe₃O₄ had a great effect on sensing performance. The reason may be that their morphology had an important impact on the surface area, active site and ion kinetics of materials, which could effectively influence its electrochemical performance. The experimental data showed that the band-shaped Fe₃O₄/rGO modified electrode exhibited high sensitivity for Pb(II) detection [38]. However, up to now, the preparation of electrochemical sensors which combine the outstanding merits of Fe₃O₄ NPs and GR for rutin determination is still scarcely reported.

In this paper, an inexpensive, rapid and efficient synthetic route is adopted for the preparation of the Fe₃O₄ NPs-GR nanocomposite. Amine-functionalized Fe₃O₄ (NH₂-Fe₃O₄ NPs) was synthesized, which could bind with GO via hydrogen bonding between the amino-groups attached to NH₂-Fe₃O₄ and the oxygen-containing groups such as hydroxyl, epoxy and carboxyl groups residing on the surface of GO, and the resulting nanocomposites had good dispersibility and stability. Then, the potentiostatic reduction of GO sheets was electrochemically employed to generate reduced graphene oxide (ErGO) on the surface of GCE. Based on this, cyclic voltammetry (CV) and second derivative linear sweep voltammetry (SDLSV) were both adopted to investigate as-fabricated NH₂-Fe₃O₄ NPs-ErGO/GCE and its sensing performances towards the rutin oxidation. The electrochemical results showed that the voltammetric response of rutin was enhanced greatly on NH₂-Fe₃O₄ NPs-ErGO/GCE. Therefore, a novel sensitive voltammetric approach for rutin determination at nanomolar level was symmetrically explored.

2. Experimental

2.1. Materials and Reagents

Rutin (C₂₇H₂₀O₁₆·3H₂O), sodium nitrate, concentrated sulfuric acid, ferric trichloride hexahydrate (FeCl₃·6H₂O), potassium permanganate, hydrogen peroxide, graphite powder, 1,2-ethylenediamine and ethylene glycol were purchased from Sinopharm Chemical Reagent Co. Ltd. (Shanghai, China). A stock solution of rutin (1.0 mM) was prepared in 50% (*v/v*) ethanol and kept at 4 °C when not in use. More dilute solutions were prepared accordingly when needed. For all electrochemical measurements, 0.2 M H₂SO₄ was used as the electrolyte. All other reagents were of analytical grade and used as received. Doubly distilled water was used throughout the study.

2.2. Characterization Apparatus

Cyclic Voltammetry (CV) was measured on a CHI 660E electrochemical workstation (Chenhua Instrument, Shanghai, China). Second derivative linear sweep voltammetry (SDLSV) was conducted on a JP-303E polarographic analyzer (Chengdu Instrument Factory, Chengdu, China). A conventional three-electrode system was used throughout the electrochemical experiments, which consisted of a working electrode (NH₂-Fe₃O₄ NPs-ErGO/GCE), a counter electrode (platinum electrode), and a reference electrode (saturated calomel electrode, SCE), respectively. The pH measurements were performed on a pH-3c exact digital pH meter (Shanghai Leichi Instrument Factory, Shanghai, China). Fourier transform infrared spectroscopy (FTIR) was recorded on Varian Excalibur 3100 spectrometer (Palo Alto, CA, USA). Scanning electron microscope (SEM) images were collected from a Hitachi S-3000N scanning electron microscope (Hitachi, Tokyo, Japan) at an acceleration potential of 30 kV. Transmission electron microscope (TEM) images were recorded from JEOL JEM-2010 (HT, Tokyo, Japan) operated at 200 kV. X-ray diffraction (XRD) patterns were operated with an X-ray diffractometer (PAN Alytical, Amsterdam, Holland). Magnetic hysteresis loop of NH₂-Fe₃O₄ NPs was detected by a vibrating sample magnetometer (VSM, Instrument Factory of Nanjing University, Nanjing, China). The ultraviolet (UV) absorption spectra were obtained on a UV-2501PC spectrophotometer (Shimadzu Co., Tokyo, Japan) in the wavelength range 200–450 nm with 1 cm matched quartz cells.

2.3. Preparation of NH₂-Fe₃O₄ NPs and GO Composites

Graphene oxide (GO) was synthesized using a modified Hummers method as reported in our previous publication [39]. Briefly, 23 mL concentrated sulfuric acid was cooled to 0 °C, and 0.5 g graphite powder, 0.5 g sodium nitrate and 3.0 g potassium permanganate were added under mechanical stirring below 5 °C. Then, the mixture was stirred for 2 h at 35 °C to form a mash. Subsequently, 40 mL water was added slowly into the solution below 50 °C, then the temperature was increased to 95 °C and the mixture was stirred for 0.5 h. After adding 100 mL of water, the above solution was poured in 20 mL of 30% H₂O₂. The suspension was treated by suction filtration, and the precipitate

was washed with 1.0 M hydrochloric acid and water, respectively. The graphite oxide was obtained by drying under 50 °C vacuum overnight. Finally, 100 mg graphite oxide were dispersed in 100 mL water and exfoliated to GO by ultrasonication for 2 h, and the golden-yellow solution was obtained after centrifugation.

NH₂-Fe₃O₄ NPs were prepared via hydrothermal method according to [40]. In brief, 1.0 g FeCl₃·6H₂O was dissolved in 20 mL ethylene glycol to form a clear solution, followed by the addition of 3.0 g sodium acetate, 0.4 g sodium hydroxide, and 10 mL 1,2-ethylenediamine. The mixture was stirred vigorously for 30 min and then sealed in a Teflon lined stainless-steel autoclave. The autoclave was heated to and maintained at 200 °C for 8 h, and allowed to cool to room temperature. The obtained black magnetite particles were washed with water for several times and then dried in vacuum. After that, 1.0 mg of NH₂-Fe₃O₄ NPs was introduced into 20 mL of GO solution (1 mg/mL) in an ultrasound bath for 2 h and the NH₂-Fe₃O₄ NPs and GO nanocomposites dispersed solution were produced.

2.4. Fabrication of the Decorated Electrodes

In order to acquire a smooth surface, the bare GCE was polished with 0.05 μm α-Al₂O₃ suspension, and then it was cleaned in ethyl alcohol and doubly distilled water by sonication, each for 2 min. A total of 5 μL of NH₂-Fe₃O₄ NPs and GO nanocomposites dispersion was dropwise added onto the GCE surface and dried under an infrared lamp. The electrode denoted as NH₂-Fe₃O₄ NPs-GO/GCE was achieved. Then, NH₂-Fe₃O₄ NPs-ErGO/GCE was fabricated by electrochemical reduction of GO in phosphate buffer solution (PBS, pH 6.5) at −1.2 V for 150 s. For comparison and further investigation, NH₂-Fe₃O₄ NPs/GCE, GO/GCE, ErGO/GCE were similarly fabricated as above-mentioned procedure.

2.5. Analytical Procedure

A total of 1.0 mL of 0.1 mM rutin, 1.0 mL of 1.0 M hydrochloric acid and 8.0 mL of water were transferred into a 10 mL electrochemical cell, and then the three-electrode system was set up. The electrochemical behavior of rutin on NH₂-Fe₃O₄ NPs-ErGO/GCE was measured by CV method, and SDLSV was used for rutin quantitative analysis because of its sensitivity and high resolution. CVs potential data were collected and recorded in the range from 0.0 to 1.0 V at a scan rate of 0.1 V/s. While SDLSVs potential data were collected and recorded from −0.3 to 1.1 V at a scan rate of 0.1 V/s similarly. All measurements were carried out at room temperature.

3. Results and Discussion

3.1. Characterization of Morphology and Structure of the Synthetic Materials

The morphologies of the synthesized materials were primarily characterized by SEM, and the images of GO (A), NH₂-Fe₃O₄ NPs (B) and NH₂-Fe₃O₄-ErGO nanocomposites (C) were obtained. As shown in Figure 1A, GO exhibited thin, wrinkled nanosheets. The typical morphology of NH₂-Fe₃O₄ NPs was clearly presented in Figure 1B, in which NH₂-Fe₃O₄ NPs exhibit a narrow size-distribution with an estimated average particle diameter of about 50 nm. The SEM image of NH₂-Fe₃O₄ NPs-ErGO in Figure 1C shows that ErGO sheets decorated with NH₂-Fe₃O₄ are stacked randomly, indicating that NH₂-Fe₃O₄ NP and ErGO are well combined. In addition, the surface morphology of NH₂-Fe₃O₄ NPs was studied by TEM. Most interestingly, these NH₂-Fe₃O₄ NPs with smooth surfaces demonstrate a mesoporous structure inside, and the porous size is around 10 nm. It is assumed that the assembling similar-surfactant structures formed via static attraction between sodium acetate (excess) and 1, 2-ethylenediamine ETH (excess) probably acted as the soft template for obtaining the novel mesoporous structure [41]. The NH₂-Fe₃O₄ NPs shows good dispersity and no obvious agglomeration is observed, plus the significantly small size and abundant pores, the specific surface area of NH₂-Fe₃O₄ NPs increases dramatically. It is well known that large specific surface

areas can provide more active sites and can absorb more analytes. Moreover, these pores also allow the electrons to transit inside their interior pore channels, which would improve electrocatalytic activity.

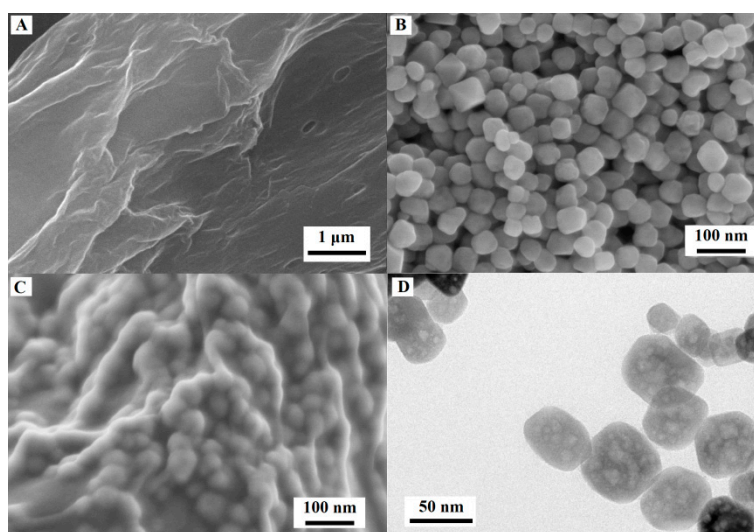


Figure 1. Scanning electron microscope (SEM) images of graphene oxide (GO) (A), Amine-functionalized Fe_3O_4 nanoparticles ($\text{NH}_2\text{-Fe}_3\text{O}_4$ NPs) (B) and $\text{NH}_2\text{-Fe}_3\text{O}_4$ -electrochemically reduced graphene oxide (ErGO) nanocomposites (C) and the Transmission electron microscope (TEM) image of $\text{NH}_2\text{-Fe}_3\text{O}_4$ NPs (D).

$\text{NH}_2\text{-Fe}_3\text{O}_4$ NPs were further characterized by FTIR, XRD and VSM separately. Figure 2A shows the FTIR spectra comparison of Fe_3O_4 NPs (curve a) and $\text{NH}_2\text{-Fe}_3\text{O}_4$ NPs (curve b). From curve b, it could be seen that the broad band in the range of $3300\text{--}3600\text{ cm}^{-1}$ was attributed to stretching vibrations of hydroxyl (-OH groups) absorbed by Fe_3O_4 NPs, and the absorption band near 3211 cm^{-1} was attributed to the -NH groups also existing in particles. The strong absorption peak at 577 cm^{-1} was caused by the stretching vibrations of the Fe-O bond in $\text{NH}_2\text{-Fe}_3\text{O}_4$ NPs. After amine-modification, the peak strength was weakened as compared with that of parent Fe_3O_4 NPs, which indicated that the modification of Fe_3O_4 NPs with - NH_2 was successful. It was evident that the XRD patterns of $\text{NH}_2\text{-Fe}_3\text{O}_4$ NPs (Figure 2B) displayed six diffraction peaks located at 2θ of 19.7° , 30.4° , 35.7° , 43.2° , 57.3° and 62.8° , respectively corresponding to the facets of (111), (220), (311), (400), (511) and (440) exactly the same as magnetite crystal structure (JSPDS01-1111, $a = 8.393\text{ \AA}$). No other impurity diffraction peaks were observed in the XRD pattern, indicating that the prepared $\text{NH}_2\text{-Fe}_3\text{O}_4$ NPs were crystalline pure. The magnetization curves of the $\text{NH}_2\text{-Fe}_3\text{O}_4$ NPs are shown in Figure 2C, and their magnetic saturation M_s values are around $80\text{ emu}\cdot\text{g}^{-1}$, quite similar to crystal magnetite NPs, demonstrating a very good soft magnetism [32].

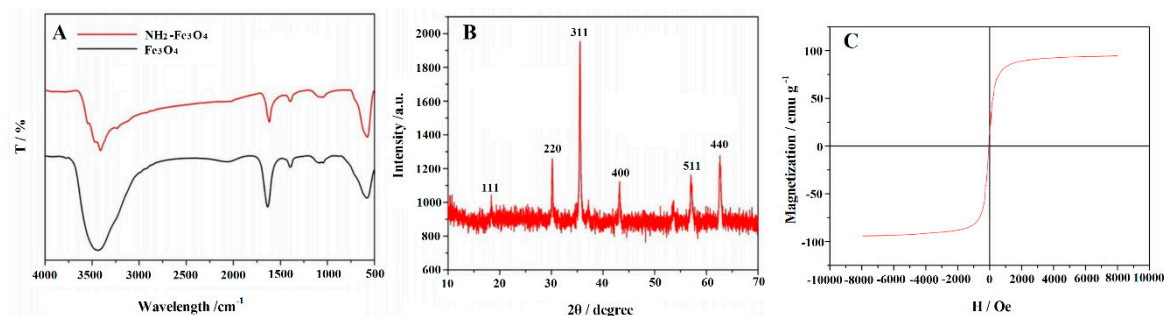


Figure 2. Fourier transform infrared spectroscopy (FTIR) spectra of Fe_3O_4 NPs and $\text{NH}_2\text{-Fe}_3\text{O}_4$ NPs (A), the X-ray diffraction (XRD) pattern of $\text{NH}_2\text{-Fe}_3\text{O}_4$ NPs (B) and the vibrating sample magnetometer (VSM) of $\text{NH}_2\text{-Fe}_3\text{O}_4$ NPs (C).

3.2. Electrochemical Properties of Modified Electrodes

The cyclic voltammetric responses on different electrodes were compared and recorded in a mixed solution of 1.0 mM $K_3[Fe(CN)_6]$ and 0.5 M KCl concentrations, as shown in Figure 3. On GCE the peak-to-peak potential separation (ΔE_p) was 79 mV and the redox peak current is the smallest (curve a), implying the quasi-reversible electron transfer process involved. However, after GO modification, there was a significant decrease of the redox peak current of $[Fe(CN)_6]^{3-/4-}$, which may be caused by the weak conductivity of GO and negative charge repulsion force between the ionized groups such as COO^- in GO and $[Fe(CN)_6]^{3-/4-}$ (curve b). While on $NH_2-Fe_3O_4$ NPs-GO/GCE (curve c) and ErGO/GCE (curve d) the redox peak currents increased gradually, which may result from the presence of $NH_2-Fe_3O_4$ NPs and ErGO on GCE surface. Moreover, the current value on ErGO/GCE was larger than that of $NH_2-Fe_3O_4$ NPs/GCE, indicating a better conductivity of ErGO nanosheets than that of $NH_2-Fe_3O_4$ NPs. On $NH_2-Fe_3O_4$ NPs-ErGO/GCE (curve e), the highest redox peak current appeared with the ΔE_p value decreased to 42 mV, implying a more reversible electron transfer process occurred for $[Fe(CN)_6]^{3-/4-}$ probe. Therefore, the coexistence of ErGO and $NH_2-Fe_3O_4$ NPs on the surface of GCE can complementarily improve the electron transfer rate and optimize a suitable electrochemical interface for the further application.

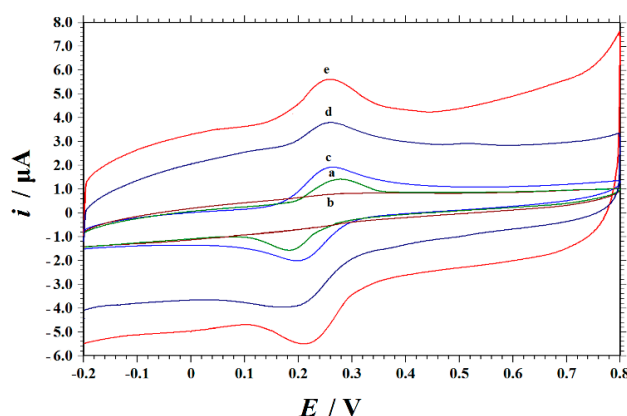


Figure 3. Cyclic voltammograms of glassy carbon electrode (GCE) (a), graphene oxide modified glassy carbon electrode (GO/GCE) (b), $NH_2-Fe_3O_4$ NPs-GO/GCE (c), ErGO/GCE (d), and $NH_2-Fe_3O_4$ NPs-ErGO/GCE (e) in 1.0 mmol/L $K_3[Fe(CN)_6]$ and 0.5 mol/L KCl with the scan rate of 0.1 V/s.

3.3. Rutin Cyclic Voltammograms on the Decorated Electrodes

The electrochemical behavior of rutin was firstly investigated by means of cyclic voltammetry (CV). Figure 4 shows the cyclic voltammograms of 10.0 μM rutin at different electrodes in 0.2 M H_2SO_4 at a scan rate of 0.1 $V s^{-1}$. A pair of redox peaks was observed at each electrode from 0.0 to 1.0 V, indicating that rutin underwent a reversible redox process. Table 1 summarized the rutin electrochemical data at various decorated electrodes. It can be seen that on GO/GCE, the redox peak currents were smaller than that of GCE (curve b), which may be due to the low conductivity of GO, resulting in delayed electron transfer. The electrochemical data showed that the redox currents of rutin on $NH_2-Fe_3O_4$ NPs-GO/GCE (curve c) and ErGO/GCE (curve d) were larger than that of bare GCE (curve a), which indicated the superiority of $NH_2-Fe_3O_4$ NPs-GO/GCE and ErGO/GCE such as large surface area, inherent electrocatalytic ability, and good conductivity towards rutin detection. While on $NH_2-Fe_3O_4$ NPs-ErGO/GCE the maximum redox peak currents appeared, indicating the synergistic effects of ErGO and $NH_2-Fe_3O_4$ NPs were present on the electrode surface. ErGO has the advantages of large specific surface area, good catalytic activity and high conductivity. While the $NH_2-Fe_3O_4$ NPs used in this experiment have excellent electrocatalytic activity and can be used as an electronic mediator to promote the transfer of electrons between the modified electrode and rutin

solution. Due to the excellent properties of ErGO and $\text{NH}_2\text{-Fe}_3\text{O}_4$ NPs combination, the sensing performance of the sensor towards rutin detection was greatly improved.

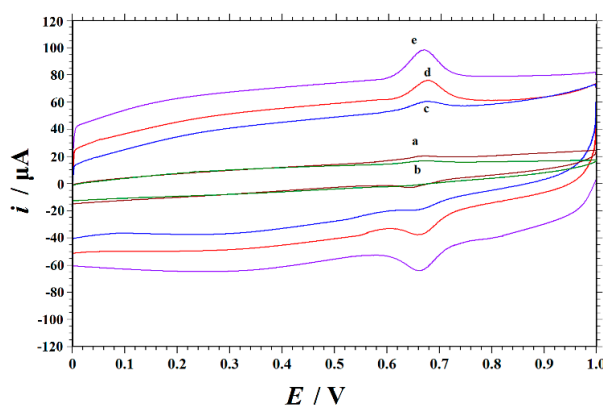


Figure 4. Cyclic voltammograms of 10.0 μM rutin on the different electrodes in 0.2 M H_2SO_4 : GCE (a), GO/GCE (b), $\text{NH}_2\text{-Fe}_3\text{O}_4$ NPs-GO/GCE (c), ErGO/GCE (d), and $\text{NH}_2\text{-Fe}_3\text{O}_4$ NPs-ErGO/GCE (e). The scan rate of 0.1 V/s.

The electrochemical behavior of rutin on various electrodes was also investigated by the method of second derivative linear sweep voltammetry (SDLSV) in order to improve the sensitivity. Figure 5 shows the corresponding voltammograms of the $\text{NH}_2\text{-Fe}_3\text{O}_4$ NPs-ErGO/GCE immersed in 10.0 μM rutin (0.2 M H_2SO_4). As it can be noticed, the oxidation peaks appear to have the same potentials as in the case of the CV. As compared to those of the CV results, the peaks obtained via SDLSV are better defined, the background current is lower, and the currents are higher. Therefore, SDLSV is the most suitable technique for rutin quantitative analysis. As shown in Figure 5, the current responses of rutin on different electrodes increased in the order of i_p (GO/GCE) (0.6250 μA) < i_p (GCE) (1.863 μA) < i_p ($\text{NH}_2\text{-Fe}_3\text{O}_4$ NPs-GO/GCE) (2.650 μA) < i_p (ErGO/GCE) (15.99 μA) < i_p ($\text{NH}_2\text{-Fe}_3\text{O}_4$ NPs-ErGO/GCE) (24.95 μA). As compared with that of GCE, the oxidation peak potential of rutin on $\text{NH}_2\text{-Fe}_3\text{O}_4$ NPs-ErGO/GCE shifted negatively by 11 mV and the oxidation peak current increased by nearly 13 times, as a result of the synergistic enhancement effect of ErGO and $\text{NH}_2\text{-Fe}_3\text{O}_4$ NPs on the electrochemical reaction of rutin.

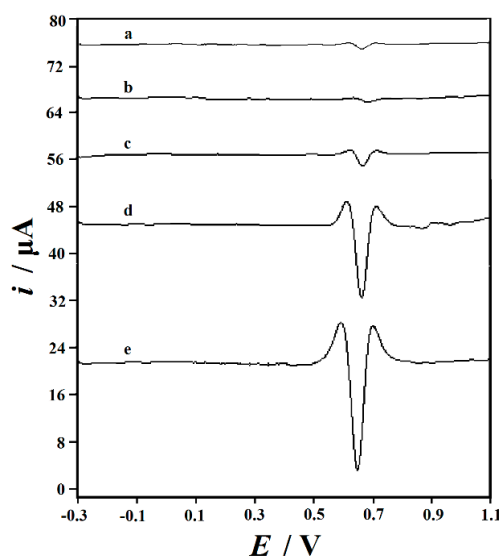


Figure 5. Second-order derivative linear scan voltammograms of 10.0 μM rutin on the different electrodes in 0.2 M H_2SO_4 after accumulation at -0.3 V for 210 s: GCE (a), GO/GCE (b), $\text{NH}_2\text{-Fe}_3\text{O}_4$ NPs-GO/GCE (c), ErGO/GCE (d), and $\text{NH}_2\text{-Fe}_3\text{O}_4$ NPs-ErGO/GCE (e). The scan rate of 0.1 V/s.

3.4. Effect of Scan Rate

Figure 6 shows the cyclic voltammograms of 10.0 μM rutin at $\text{NH}_2\text{-Fe}_3\text{O}_4$ NPs-ErGO/GCEABPE with different scan rates (0.03–0.3V/s). As exhibited in Figure 6A, a pair of roughly symmetric anodic and cathodic peaks appeared, the rutin peak currents increased as the scan rate (v) increased and a significant linear relationship is observed between the peak currents and scan rates (Figure 6B). The regression equation is $i_{\text{pa}} (\mu\text{A}) = 253.01 v (\text{V/s}) - 6.4469$ ($R^2 = 0.9958$) and $i_{\text{pc}} (\mu\text{A}) = -187.86v (\text{V/s}) + 4.9146$ ($R^2 = 0.9931$), indicating that the electrode process of rutin on $\text{NH}_2\text{-Fe}_3\text{O}_4$ NPs-ErGO/GCE is controlled by adsorption. However, there was no significant change in the peak potentials with increasing the scan rate, which confirmed that the electrochemical reaction of rutin is reversible on the surface of $\text{NH}_2\text{-Fe}_3\text{O}_4$ NPs-ErGO/GCE.

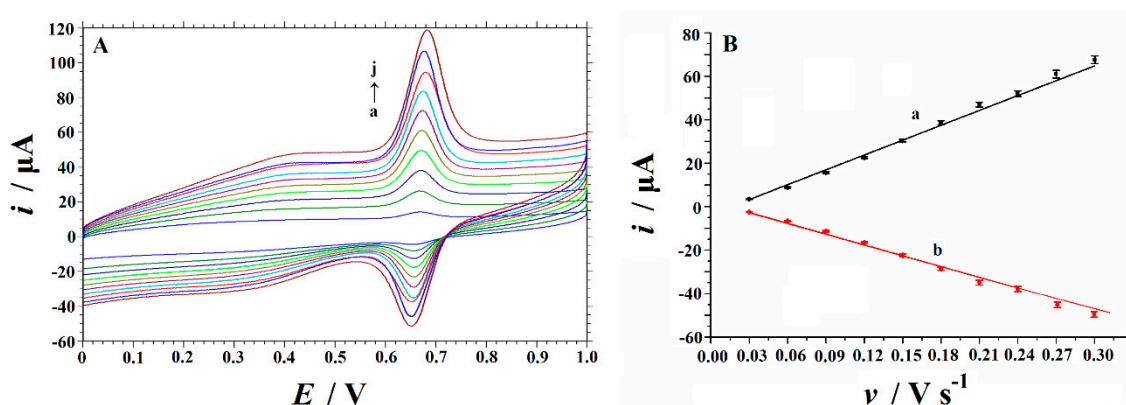


Figure 6. (A) Cyclic voltammograms of 10 μM rutin in 0.1 mol L^{-1} HCl solution on $\text{NH}_2\text{-Fe}_3\text{O}_4$ NPs-ErGO/GCE at various scan rates (Form a to j: 0.03, 0.06, 0.09, 0.12, 0.15, 0.18, 0.21, 0.24, 0.27, 0.3 V s^{-1} , respectively); (B) Plot of oxidation peak currents (a) and reduction peak currents (b) versus scan rates.

3.5. Effects of Supporting Electrolyte and Solution pH Variation

In general, supporting electrolyte and the pH of buffer solution play a dominant role for the voltammetric response of electrochemically active substances. To understand the effect of supporting electrolyte, SDLSVs were recorded and compared in many buffer solutions including HAc–NaAc buffer (pH 4.0), HAc– NH_4Ac buffer (pH 4.0), phosphate buffer (pH 6.0), $(\text{CH}_2)_6\text{N}_4\text{-HCl}$ buffer (pH 5.0), $\text{NH}_3\text{-NH}_4\text{Cl}$ (pH 9.0), H_2SO_4 , HNO_3 , HCl and NaOH, each 0.1 M), respectively. The experimental data in Table 2 proved that the electro-oxidation of rutin is better performed in acidic media, while in neutral or alkaline media, the peak current decreased considerably. These phenomena might be explained by the fact that the hydroxyl groups in the rutin structure lost their protons in the basic solution, so the electrochemical reaction of rutin was more difficult to achieve [14,42]. The highest peak current and the best peak shape were observed in H_2SO_4 solution, thus it was selected as the working media.

From Figure 7, it can be seen that the oxidation peak current of rutin increased with the increase of H_2SO_4 concentration from 0.01 to 0.2 M, and then decreased with further increasing the concentration from 0.2 to 0.7 M. The maximum peak current appeared at 0.2 M concentration of H_2SO_4 . The influence of pH on the peak potential of rutin was also studied. By changing the concentrations of H_2SO_4 , different pH values media were obtained. As the value of the pH rises, a linear movement towards the lower peak potential values can be observed, and corresponding regression equation is $E_{\text{pa}} (\text{V}) = -0.0556 \text{ pH} + 0.6528$ ($R^2 = 0.9862$). The slope between the peak potential and the pH is -55.6 mV/pH units, indicating that an equal number of electrons and protons are involved in the redox process as same as reported previously [43]. According to [13,14,42], the mechanism of electrooxidation of rutin could be explained as that the catechol structure of rutin is oxidized to 3',4'-diquinone, and the reduction reaction could take place on the decorated electrode surface. The electrode reaction equation was illustrated as the following Scheme 1.

Table 2. Effect of different supporting electrolytes (0.1 M) on the current and potential response of 10 μM rutin at $\text{NH}_2\text{-Fe}_3\text{O}_4$ NPs-ErGO/GCE. Accumulation time: 30 s, other conditions are the same as in Figure 5.

| Electrolyte | Peak Current (μA) | Peak Potential (V) |
|--|--------------------------------|--------------------|
| HAc-NaAc buffer (pH 4.0) | 4.275 | 0.540 |
| HAc-NH ₄ Ac (pH 4.0) | 4.645 | 0.564 |
| (CH ₂) ₆ N ₄ -HCl (pH 5.0) | 3.688 | 0.528 |
| phosphate buffer (pH 6.0) | 3.951 | 0.480 |
| NH ₃ -NH ₄ Cl (pH 9.0) | 1.264 | 0.432 |
| HCl | 6.200 | 0.648 |
| HNO ₃ | 6.418 | 0.660 |
| H ₂ SO ₄ | 6.863 | 0.664 |
| NaOH | 0.645 | 0.328 |

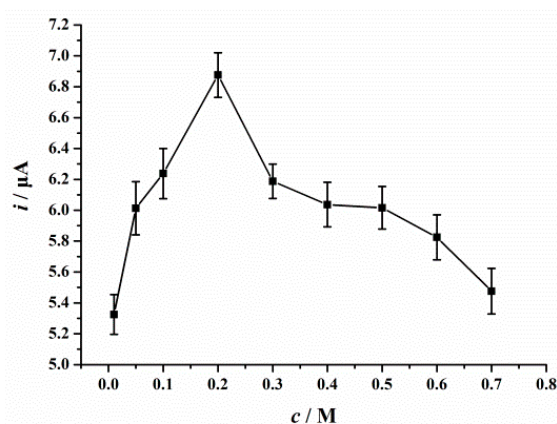
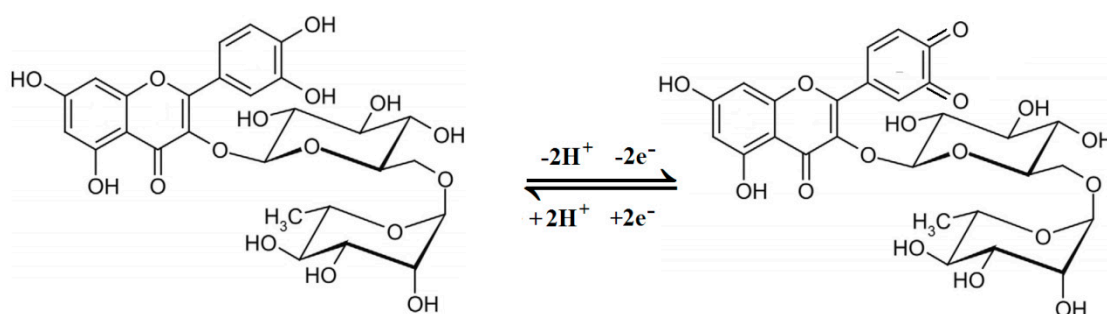


Figure 7. The dependence relationship of the peak current of 10 μM rutin and H_2SO_4 concentration by SDLSV, error bars represent SD, $n = 3$. Accumulation potential: -0.3 V, accumulation time: 30 s, scan rate of 0.1 V/s.



Scheme 1. Electrochemical reaction mechanism of rutin.

3.6. Optimization of Parameters

3.6.1. Electrochemical Reduction Conditions

It is well known that pure GR sometimes fails to demonstrate perfect performance because oxygen-contaminated functional groups (OxFG) often play a leading role of catalytic active centers in electrochemical reactions as reported [44,45]. The potentiostatic reduction method is easy to control. By changing the potential and time of reduction, a certain number of OxFG can remain [44]. In this work, GO was reduced by potentiostatic method. The $\text{NH}_2\text{-Fe}_3\text{O}_4$ NPs-ErGO/GCE was immersed and reduced in phosphate buffer (pH 6.5) under adjusting potentials (-0.8 , -1.0 , -1.2 , -1.5 , and -1.7 V, respectively) for 120 s. After that, the oxidation peak currents of 10 μM rutin were measured and compared. The results showed that the peak current of rutin increased with the decrease of reduction

potential, from -0.8 to -1.2 V. However, the peak current decreased when the reduction potential shifted to more negative direction (Figure 8A). The effect of reduction time was also investigated at a constant reduction potential of -1.2 V (Figure 8B). The peak current increased greatly within the first 150 s and then declined gradually. Consequently, -1.2 V and 150 s were used for the electrochemical optimum conditions for GO reduction.

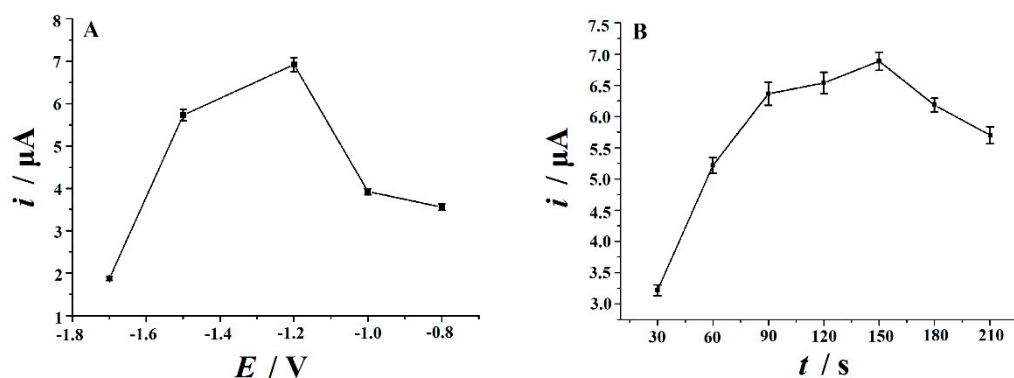


Figure 8. (A) Effect of reduction potential and (B) reduction time on the peak current of $10 \mu\text{M}$ rutin in $0.2 \text{ M H}_2\text{SO}_4$ at $\text{NH}_2\text{-Fe}_3\text{O}_4$ NPs-ErGO/GCE by second derivative linear sweep voltammetry (SDLSV). Other conditions are the same as in Figure 7.

3.6.2. Accumulation Conditions

To enrich rutin concentration onto the $\text{NH}_2\text{-Fe}_3\text{O}_4$ NPs-ErGO/GCE surface, accumulation was carried out before its detection. The effect of accumulation potential and time on the oxidation peak current (i_{pa}) were examined. After 30 s accumulation time, the i_{pa} was recorded at varying accumulation potentials in the range from -0.4 to 0.3 V. As shown in Figure 9A, the highest i_{pa} appeared at the accumulation potential of -0.3 V. What is more, the effect of accumulation time was studied and compared at a fixed accumulation potential of -0.3 V (Figure 9B). In the first 270 s, with the increase of accumulation time, the i_{pa} increased significantly, and then with the further increase of accumulation time, the i_{pa} remained basically unchanged, indicating that the adsorption reached saturation. However, it is inconvenient using a long accumulation time. Therefore, the accumulation time of 210 s was used as a compromise between analysis speed and sensitivity.

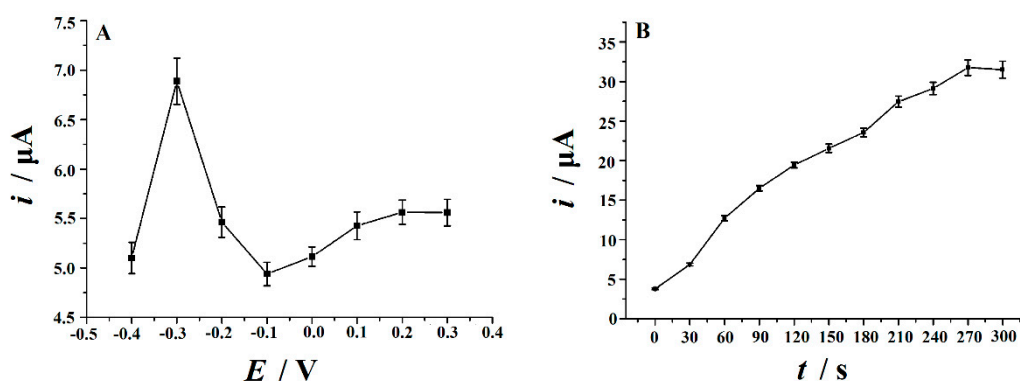


Figure 9. (A) Accumulation potential effects and (B) accumulation time effects on the peak current of $10 \mu\text{M}$ rutin in $0.2 \text{ M H}_2\text{SO}_4$ at $\text{NH}_2\text{-Fe}_3\text{O}_4$ NPs-ErGO/GCE by SDLSV.

3.7. Figures of Merit

3.7.1. The Study of Interferences

In order to facilitate the application, the effects of some foreign substances, especially those that commonly co-exist in biological samples and the pharmaceutical formulations, on the rutin detection were investigated by SDLSV. The interference study was performed by immersing the $\text{NH}_2\text{-Fe}_3\text{O}_4$ NPs-ErGO/GCE into a fixed concentration of 1.0 μM rutin solution mixed with added foreign species. The results demonstrated that the relative error (RE) after adding interfering substances was less than $\pm 5.0\%$, which indicated that $\text{NH}_2\text{-Fe}_3\text{O}_4$ NPs-ErGO/GCE has good anti-interference ability for rutin determination (Table 3).

Table 3. Influence of co-existing substances on the determination of 1.0 μM rutin ($n = 3$).

| Coexisting Substance | Concentration/mM | Change of Peak Current/ μA | RE/% | Coexisting Substance | Concentration/mM | Change of Peak Current/ μA | RE/% |
|----------------------|------------------|---------------------------------------|-------|----------------------|------------------|---------------------------------------|-------|
| glucose | 1 | 0.0546 | 1.28 | uric acid | 0.1 | 0.1761 | 4.13 |
| citric acid | 1 | 0.0674 | 1.58 | Mn^{2+} | 1 | -0.0942 | -2.21 |
| glutamate | 1 | 0.1006 | 2.36 | Zn^{2+} | 1 | 0.1530 | 3.59 |
| arginine | 1 | 0.1351 | 3.17 | Ca^{2+} | 1 | -0.1343 | -3.15 |
| tryptophan | 0.1 | 0.1842 | 4.32 | Mg^{2+} | 1 | -0.0840 | -1.97 |
| tyrosine | 0.1 | 0.1543 | 3.62 | Pb^{2+} | 1 | 0.1100 | 2.58 |
| glycine | 1 | 0.0503 | 1.18 | Cu^{2+} | 1 | 0.1778 | 4.17 |
| lactose | 1 | 0.0678 | 1.59 | Al^{3+} | 1 | -0.0972 | -2.28 |
| lactic acid | 1 | 0.1006 | 2.36 | K^+ | 1 | -0.0495 | 1.16 |
| starch | 1 | -0.1215 | -2.85 | Na^+ | 1 | 0.0622 | 1.46 |
| sucrose | 1 | 0.1177 | 2.76 | PO_4^{3-} | 1 | 0.0925 | 2.17 |
| dopamine | 1 | 0.2063 | 4.84 | NO_3^- | 1 | 0.0674 | 1.58 |
| ascorbic acid | 1 | -0.1253 | -2.94 | Cl^- | 1 | -0.0657 | -1.54 |

In addition, ascorbic acid (AA) is a chemically electroactive substance which often coexists with rutin in plants, crude drugs, pharmaceutical preparations (especially compound rutin tablets) and other biological samples. What is worse, the oxidation peak potential of AA is very close to that of rutin, indicating a poor selectivity and serious interfering effect for the rutin detection in real samples [19,20]. Therefore, the electrochemical responses of rutin in the presence of AA on the $\text{NH}_2\text{-Fe}_3\text{O}_4$ NPs-ErGO/GCE were studied. The typical SDLSVs of 10.0 μM rutin in the absence and presence of AA on $\text{NH}_2\text{-Fe}_3\text{O}_4$ NPs-ErGO/GCE is shown in Figure 10. A well defined oxidation peak at 0.665 V was found for rutin (curve a). Curve b is the voltammogram of 10.0 μM rutin in the presence of 1.0 mM AA under the same conditions. Two oxidation peaks of AA and rutin correspond to those at 0.296 and 0.665 V respectively. Thus, the oxidation peak potential separation was calculated as 0.369 V. The results show that a 100-fold excess of AA had no substantial interfering effect on the rutin determination (RE = -2.94%).

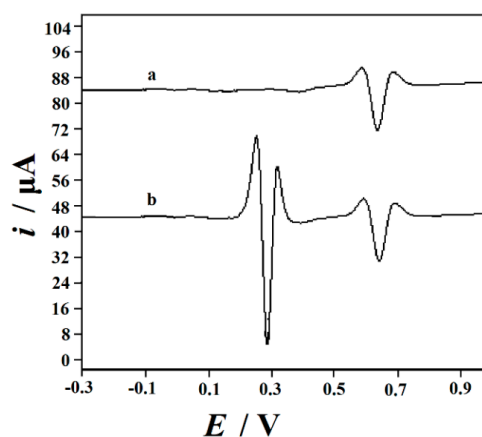


Figure 10. Second-order derivative linear scan voltammograms of 10 μM rutin in the absence of ascorbic acid (AA) (a) and in the presence of 1.0 mM AA (b) on $\text{NH}_2\text{-Fe}_3\text{O}_4$ NPs-ErGO/GCE in 0.1 M HCl after a 120 s accumulation at -0.3V . Scan rate is 0.1 V s^{-1} .

3.7.2. Calibration and Detection Limit

Under the optimized conditions and parameters, the calibration curve of rutin detection was established by SDLSV technique due to its better sensitivity and well-separated peak shape. The i_{pa} value of rutin increased gradually with the increment of rutin concentration. As plotted in Figure 11, the linear relationships were established in three sections from the range of 6.0 nM–0.1 μ M; 0.1–8.0 μ M and 8.0–80 μ M, the linear regression equations were $i_p (\mu\text{A}) = 7.3324c (\mu\text{M}) + 0.2308$ ($R^2 = 0.9986$), $i_p (\mu\text{A}) = 2.8677c (\mu\text{M}) + 1.0583$ ($R^2 = 0.9984$), and $i_p (\mu\text{A}) = 0.6752c (\mu\text{M}) + 20.021$ ($R^2 = 0.9982$), respectively. A low detection limit of 4.0 nM was achieved. It is found that the calibration dependences exhibit intersection of calibration lines and the slopes are decreasing with increasing concentration of rutin. This phenomenon is caused by the fact that the peak current of rutin increases rapidly at low concentrations, and then increases slowly at higher concentrations. This may be explained with the saturated adsorption of rutin on the electrode surface and the rising of diffusion current at higher concentrations.

The method reported hereby and some previous procedures for rutin analysis are compared and summarized in Table 4 in terms of analytical figures and merits. As listed in Table 4, the proposed method can provide a linear range and detection limit comparable to (even superior to) other methods. In addition, this novel method has made remarkable progress in electrode fabrication simplification, time-saving and cost-reduction.

Table 4. Comparisons among various electrochemical methods for rutin detection.

| Electrochemical Sensors | Technique | Supporting Electrolyte | Linear Range/ μ M | Correlation Coefficient | Detection Limit/ μ M | References |
|--|------------------|--------------------------------------|-----------------------------|-------------------------|--------------------------|------------|
| ^a GR–AuNPs/CSPE | ^j SWV | HAc–NaAc buffer (pH 5.0) | 0.1–15 | 0.9988 | 0.011 | [12] |
| ^b GR/CILE | ^k DPV | PBS buffer (pH 2.5) | 0.07–10; 10–100 | 0.997, 0.991 | 0.024 | [13] |
| ^c Cu–CS/MWCNT/GCE | DPV | B–R buffer (pH 3) | 0.05–100 | 0.9994 | 0.01 | [14] |
| ^d BP–PEDOT:PSS/GCE | DPV | PBS buffer (pH 2.5) | 0.02–15.0; 15.0–80.0 | 0.998, 0.996 | 0.007 | [15] |
| ^e GR–MnO ₂ /CILE | DPV | PBS buffer (pH 2.5) | 0.01–500.0 | 0.992 | 0.00273 | [16] |
| ^f AgNPs/PMB–GR/Au electrode | DPV | PBS buffer (pH 3.0) | 0.01–0.1; 0.1–2.0; 2.0–10.0 | 0.9947, 0.9959, 0.9958 | 0.01 | [17] |
| ^g IL/CPE | SWV | B–R buffer (pH 3.29) | 0.04–10 | 0.9984 | 0.01 | [18] |
| ^h MWCNTs–CHIT/ABPE | SDLSV | 0.1 M HCl | 0.02–10 | 0.9994 | 0.01 | [19] |
| ⁱ CTAB/ABPE | SDLSV | 0.1 M HCl | 0.006–0.2; 0.2–10 | 0.9985, 0.9992 | 0.004 | [20] |
| NH ₂ –Fe ₃ O ₄ NPs–ErGO/GCE | SDLSV | 0.2 M H ₂ SO ₄ | 0.006–0.1; 0.1–8.0; 8.0–80 | | 0.004 | This work |

^a graphene-gold nanoparticle carbon screen printed electrode; ^b graphene modified carbon ionic liquid electrode; ^c chemically cross-linked copper-complexed chitosan/multi-walled carbon nanotubes modified glassy carbon electrode; ^d black phosphorene- poly(3,4-ethylenedioxythiophene)-poly(styrenesulfonate) modified glassy carbon electrode; ^e graphene-MnO₂ nanocomposite modified carbon ionic liquid electrode; ^f Ag nanoparticles/poly(methylene blue) functionalized graphene composite film modified Au electrode; ^g ionic liquid modified carbon paste electrode; ^h multi-walled carbon nanotubes–chitosan composite film modified acetylene black paste electrode; ⁱ cetyltrimethyl ammonium bromide film modified acetylene black paste electrode; ^j square-wave voltammetry; ^k differential pulse voltammetry.

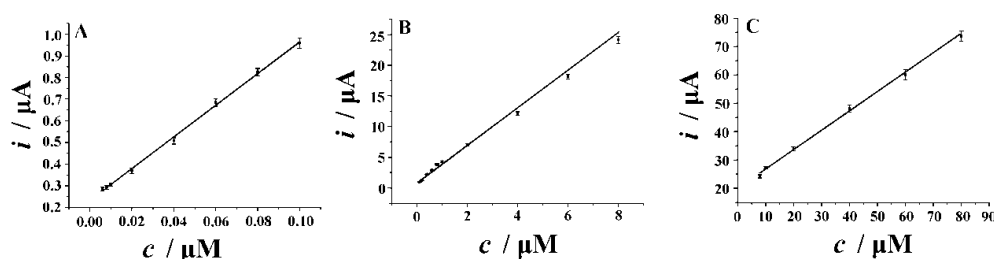


Figure 11. Plot of the peak current versus the concentration of rutin in the range from 6.0nM–0.1 μ M (A); 0.1–8.0 μ M (B) and 8.0–80 μ M (C). Accumulation potential: -0.3 V, accumulation time: 210 s, scan rate of 0.1 V/s.

3.7.3. Repeatability and Stability of the Decorated Electrode

The repeatability of the $\text{NH}_2\text{-Fe}_3\text{O}_4$ NPs-ErGO/GCE was evaluated by detecting 10 μM rutin. The relative standard deviation (RSD) of peak current measured for seven consecutive times was 2.7%. Six different electrodes were fabricated under the same procedure and the reproducibility was also tested. The RSD was 6.2% for the peak current of 10 μM rutin. The stability of the modified electrode was also examined. The electrode was stored at 4 °C in a refrigerator when not in use, and the current response of 10 μM rutin on the electrode remained 92.1% (RSD = 2.7%, $n = 3$) of its initial value after a week. These results indicated that the modified electrode had good regeneration performance and stability.

3.8. Analytical Application

Compound rutin tablets (20 mg per tablet, Shanxi Yunpeng Pharmaceutical Co. Ltd., China; Shanxi Linfen Qilin Pharmaceutical Co. Ltd., Linfen, China) and urine samples from volunteers were detected in order to evaluate the reliability in practical application of the developed method. Five pieces of rutin tablets were ground into powder in an agate mortar, and then the accurate weight of one tablet was weighed, dissolved with absolute alcohol and diluted to 10.0 mL to obtain the stock solution. Subsequently, an appropriate amount of the stock solutions and urine samples were diluted with 0.1 M HCl by different factors as the testing solution. Electrochemical test was performed under the optimal experimental conditions by SDLSV and the recoveries were obtained by the standard addition method. As summarized in Table 5, the results were satisfactory with the recoveries in the range of 98.8–103.7% for tablet samples and 101.4–103.0% for urine samples, respectively. UV-vis spectrophotometry was selected as a reference method to assess the accuracy of the proposed method. The *t*-test implied that there is no significant difference when the results are at a 99% confidence level, which proved that the voltammetric method for rutin detection is precisely accurate for real sample analysis.

Table 5. Rutin detection results from compound rutin tablets and urine samples ($n = 4$).

| Sample | Labelled/ μM | ^d Detected by UV Method/ μM | ^d Detected by this method/ μM | Added/ μM | ^d Total Found by this Method/ μM | Recovery/% |
|-----------------------|-------------------------|---|---|----------------------|--|------------|
| ^a Tablet 1 | 32.76 | 32.95 \pm 0.94 | 31.48 \pm 0.86 | 30.00 | 61.13 \pm 2.14 | 98.8 |
| ^b Tablet 2 | 3.28 | 3.08 \pm 0.11 | 3.37 \pm 0.15 | 3.00 | 6.48 \pm 0.20 | 103.7 |
| Urine 1 ^c | - | ^e ND | ND | 5.00 | 5.07 \pm 0.18 | 101.4 |
| Urine 2 ^c | - | ND | ND | 1.00 | 1.03 \pm 0.03 | 103.0 |

^a Dilution factor: 1/100; ^b Dilution factor: 1/1000; ^c Dilution factor: 1/10; ^d Average \pm confidence interval, the confidence level is 95%; ^e Not detected.

4. Conclusions

Herein, a feasible and reliable electrochemical sensor for the detection of rutin was developed using a nanocomposite of amine-functionalized Fe_3O_4 nanoparticles and electrochemically reduced graphene ($\text{NH}_2\text{-Fe}_3\text{O}_4$ NPs-ErGO) as the sensing material. Compared with bare GCE, ErGO/GCE and $\text{NH}_2\text{-Fe}_3\text{O}_4$ NPs-GO/GCE, the oxidation signals of rutin are significantly enhanced on the nanocomposites modified GCE ($\text{NH}_2\text{-Fe}_3\text{O}_4$ NPs-ErGO/GCE). Moreover, this modified electrode has been employed successfully to eliminate the interferences of ascorbic acid. The linear range for the detection of rutin using $\text{NH}_2\text{-Fe}_3\text{O}_4$ NPs-ErGO/GCE were 6.0 nM–0.1 μM ; 0.1–8.0 μM and 8.0–80 μM . The detection limit was 4.0 nM ($S/N = 3$). The developed method is sensitive and selective for the determination of rutin in pharmaceutical tablets and urine samples. Moreover, this novel method has some obvious advantages such as quick response, simplicity, high sensitivity and low cost.

Author Contributions: Q.H., P.D. and D.C. conceived and designed the experiments; Y.W., Y.T., J.L. and P.D. performed the experiments; P.D. and G.L. analyzed the data; Q.H. and D.C. contributed reagents/materials/analysis tools; Q.H. and P.D. wrote the paper.

Funding: This work was supported by the NSFC (61703152), Hunan Provincial Natural Science Foundation (2016JJ4010, 2018JJ3134), Postgraduates Innovation Fund of School of Life Science and Chemistry in HUT, Doctoral Program Construction of Hunan University of Technology, Project of Science and Technology Department of Hunan Province (Quanguo He), Project of Science and Technology Plan in Zhuzhou (201706-201806) and Opening Project of Key Discipline of Materials Science in Guangdong (ESI Project GS06021, CNXY2017001, CNXY2017002 and CNXY2017003), The key Project of Department of Education of Guangdong Province (2016GCZX008) and The Project of Engineering Research Center of Foshan (20172010018).

Conflicts of Interest: The authors declare no conflict of interest.

References

1. Tian, Q.; Li, D.; Patil, B.S. Identification and determination of flavonoids in buckwheat (*Fagopyrum esculentum* Moench, Polygonaceae) by high-performance liquid chromatography with electrospray ionisation mass spectrometry and photodiode array ultraviolet detection. *Phytochem. Anal.* **2002**, *13*, 251–256. [[CrossRef](#)] [[PubMed](#)]
2. Koval'skii, I.V.; Krasnyuk, I.I.; Nikulina, O.I.; Belyatskaya, A.V.; Kharitonov, Y.Y.; Feldman, N.B.; Lutsenko, S.V. Mechanisms of rutin pharmacological action (review). *Pharm. Chem. J.* **2014**, *48*, 73–76. [[CrossRef](#)]
3. Sharma, S.; Ali, A.; Ali, J.; Sahni, J.K.; Baboota, S. Rutin: Therapeutic potential and recent advances in drug delivery. *Expert Opin. Investig. Drugs* **2013**, *22*, 1063–1079. [[CrossRef](#)] [[PubMed](#)]
4. Wu, H.; Chen, M.; Fan, Y.; Elsebaei, F.; Zhu, Y. Determination of rutin and quercetin in Chinese herbal medicine by ionic liquid-based pressurized liquid extraction-liquid chromatography-chemiluminescence detection. *Talanta* **2012**, *88*, 222–229. [[CrossRef](#)] [[PubMed](#)]
5. Yıldırım, S.; Kadioğlu, A.; Sağlam, A.; Yaşar, A. Determination of phenolic acids and rutin in *Heliotropium thermophilum* by high-performance liquid chromatography with photodiode array detection. *Instrum. Sci. Technol.* **2017**, *45*, 35–48. [[CrossRef](#)]
6. Song, Z.; Hou, S. Sensitive determination of sub-nanogram amounts of rutin by its inhibition on chemiluminescence with immobilized reagents. *Talanta* **2002**, *57*, 59–67. [[CrossRef](#)]
7. Du, J.; Li, Y.; Lu, J. Flow injection chemiluminescence determination of rutin based on its enhancing effect on the luminol-ferricyanide/ferrocyanide system. *Anal. Lett.* **2001**, *34*, 1741–1748. [[CrossRef](#)]
8. Memon, A.F.; Solangi, A.R.; Memon, S.Q.; Mallah, A.; Memon, N.; Memon, A.A. Simultaneous determination of quercetin, rutin, naringin, and naringenin in different fruits by capillary zone electrophoresis. *Food Anal. Methods* **2017**, *10*, 83–91. [[CrossRef](#)]
9. Xu, H.; Li, Y.; Tang, H.W.; Liu, C.M.; Wu, Q.S. Determination of rutin with UV-vis spectrophotometric and laser-induced fluorimetric detections using a non-scanning spectrometer. *Anal. Lett.* **2010**, *43*, 893–904. [[CrossRef](#)]
10. Lu, Y.; Gao, B.; Chen, P.; Charles, D.; Yu, L. Characterisation of organic and conventional sweet basil leaves using chromatographic and flow-injection mass spectrometric (FIMS) fingerprints combined with principal component analysis. *Food Chem.* **2014**, *154*, 262–268. [[CrossRef](#)]
11. Duan, L.; Yang, L.; Xiong, H.; Zhang, X.; Wang, S. Studies on the electrochemistry of rutin and its interaction with bovine serum albumin using a glassy carbon electrode modified with carbon-coated nickel nanoparticles. *Microchim. Acta* **2013**, *180*, 355–361. [[CrossRef](#)]
12. Apetrei, I.M.; Apetrei, C. A modified nanostructured graphene-gold nanoparticle carbon screenprinted electrode for the sensitive voltammetric detection of rutin. *Measurement* **2018**, *114*, 37–43. [[CrossRef](#)]
13. Gao, F.; Qi, X.; Cai, X.; Wang, Q.; Gao, F.; Sun, W. Electrochemically reduced graphene modified carbon ionic liquid electrode for the sensitive sensing of rutin. *Thin Solid Films* **2012**, *520*, 5064–5069. [[CrossRef](#)]
14. Gholivand, M.B.; Mohammadi-Behzad, L.; Hosseinkhani, H. Application of a Cu-chitosan/multiwalled carbon nanotube film-modified electrode for the sensitive determination of rutin. *Anal. Biochem.* **2016**, *493*, 35–43. [[CrossRef](#)] [[PubMed](#)]

15. Niu, X.; Weng, W.; Yin, C.; Niu, Y.; Li, G.; Dong, R.; Men, Y.; Sun, W. Black phosphorene modified glassy carbon electrode for the sensitive voltammetric detection of rutin. *J. Electroanal. Chem.* **2018**, *811*, 78–83. [[CrossRef](#)]
16. Sun, W.; Wang, X.; Zhu, H.; Sun, X.; Shi, F.; Li, G.; Sun, Z. Graphene-MnO₂ nanocomposite modified carbon ionic liquid electrode for the sensitive electrochemical detection of rutin. *Sens. Actuators B* **2013**, *178*, 443–449. [[CrossRef](#)]
17. Yang, S.; Li, G.; Zhao, J.; Zhu, H.; Qu, L. Electrochemical preparation of Ag nanoparticles/poly(methylene blue) functionalized graphene nanocomposite film modified electrode for sensitive determination of rutin. *J. Electroanal. Chem.* **2014**, *717–718*, 225–230. [[CrossRef](#)]
18. Zhang, Y.; Zheng, J. Sensitive voltammetric determination of rutin at an ionic liquid modified carbon paste electrode. *Talanta* **2008**, *77*, 325–330. [[CrossRef](#)]
19. Deng, P.; Xu, Z.; Li, J. Simultaneous determination of ascorbic acid and rutin in pharmaceutical preparations with electrochemical method based on multi-walled carbon nanotubes-chitosan composite film modified electrode. *J. Pharm. Biomed. Anal.* **2013**, *76*, 234–242. [[CrossRef](#)]
20. Deng, P.; Xu, Z.; Feng, Y. Highly sensitive and simultaneous determination of ascorbic acid and rutin at an acetylene black paste electrode coated with cetyltrimethyl ammonium bromide film. *J. Electroanal. Chem.* **2012**, *683*, 47–54. [[CrossRef](#)]
21. Park, S.; Ruoff, R.S. Chemical methods for the production of graphenes. *Nat. Nanotechnol.* **2009**, *4*, 217–224. [[CrossRef](#)]
22. He, Q.; Liu, J.; Liu, X.; Li, G.; Deng, P.; Liang, J. Manganese dioxide Nanorods/electrochemically reduced graphene oxide nanocomposites modified electrodes for cost-effective and ultrasensitive detection of Amaranth. *Colloids Surf. B Biointerfaces* **2018**, *172*, 565–572. [[CrossRef](#)] [[PubMed](#)]
23. He, Q.; Liu, J.; Liu, X.; Li, G.; Chen, D.; Deng, P.; Liang, J. A promising sensing platform toward dopamine using MnO₂ nanowires/electro-reduced graphene oxide composites. *Electrochim. Acta* **2019**, *296*, 683–692. [[CrossRef](#)]
24. He, Q.; Liu, J.; Liang, J.; Liu, X.; Li, W.; Liu, Z.; Ding, Z.; Tuo, D. Towards Improvements for Penetrating the Blood–Brain Barrier—Recent Progress from a Material and Pharmaceutical Perspective. *Cells* **2018**, *7*, 24. [[CrossRef](#)] [[PubMed](#)]
25. He, Q.; Liu, J.; Liu, X.; Li, G.; Deng, P.; Liang, J.; Chen, D. Sensitive and Selective Detection of Tartrazine Based on TiO₂-Electrochemically Reduced Graphene Oxide Composite-Modified Electrodes. *Sensors* **2018**, *18*, 1911. [[CrossRef](#)] [[PubMed](#)]
26. He, Q.; Liu, J.; Liu, X.; Xia, Y.; Li, G.; Deng, P.; Chen, D. Novel Electrochemical Sensors Based on Cuprous Oxide-Electrochemically Reduced Graphene Oxide Nanocomposites Modified Electrode toward Sensitive Detection of Sunset Yellow. *Molecules* **2018**, *23*, 2130. [[CrossRef](#)] [[PubMed](#)]
27. He, Q.; Liu, J.; Liu, X.; Li, G.; Chen, D.; Deng, P.; Liang, J. Fabrication of Amine-Modified Magnetite-Electrochemically Reduced Graphene Oxide Nanocomposite Modified Glassy Carbon Electrode for Sensitive Dopamine Determination. *Nanomaterials* **2018**, *8*, 194. [[CrossRef](#)] [[PubMed](#)]
28. Ning, J.; He, Q.; Luo, X.; Wang, M.; Liu, D.; Wang, J.; Li, G.; Liu, J. Determination of Uric Acid in Co-Presence of Dopamine and Ascorbic Acid Using Cuprous Oxide Nanoparticle-Functionalized Graphene Decorated Glassy Carbon Electrode. *Catalysts* **2018**, *8*, 407. [[CrossRef](#)]
29. Ning, J.; He, Q.; Luo, X.; Wang, M.; Liu, D.; Wang, J.; Liu, J.; Li, G. Rapid and Sensitive Determination of Vanillin Based on a Glassy Carbon Electrode Modified with Cu₂O-Electrochemically Reduced Graphene Oxide Nanocomposite Film. *Sensors* **2018**, *18*, 2762. [[CrossRef](#)]
30. He, Q.; Liu, J.; Liu, X.; Li, G.; Deng, P.; Liang, J. Preparation of Cu₂O-reduced graphene nanocomposite modified electrodes towards ultrasensitive dopamine detection. *Sensors* **2018**, *18*, 199. [[CrossRef](#)]
31. He, Q.; Liu, J.; Liang, J.; Liu, X.; Tuo, D.; Li, W. Chemically surface tunable solubility parameter for controllable drug delivery—an example and perspective from hollow PAA-coated magnetite nanoparticles with R6G model drug. *Materials* **2018**, *11*, 247. [[CrossRef](#)]
32. He, Q.; Liu, J.; Liang, J.; Liu, X.; Ding, Z.; Tuo, D.; Li, W. Sodium acetate orientated hollow/mesoporous magnetite nanoparticles: Facile synthesis, characterization and formation mechanism. *Appl. Sci.* **2018**, *8*, 292. [[CrossRef](#)]
33. Liu, J.; Huang, C.; He, Q. Pharmaceutical application of magnetic iron oxide nanoparticles. *Sci. Adv. Mater.* **2015**, *7*, 672–685. [[CrossRef](#)]

34. Ye, Y.; Kong, T.; Yu, X.; Wu, Y.; Zhang, K.; Wang, X. Enhanced nonenzymatic hydrogen peroxide sensing with reduced graphene oxide/ferroferric oxide nanocomposites. *Talanta* **2012**, *89*, 417–421. [[CrossRef](#)] [[PubMed](#)]
35. Zhang, W.; Zheng, J.; Shi, J.; Lin, Z.; Huang, Q.; Zhang, H.; Wei, C.; Chen, J.; Hu, S.; Hao, A. Nafion covered core-shell structured Fe₃O₄@graphene nanospheres modified electrode for highly selective detection of dopamine. *Anal. Chim. Acta* **2015**, *853*, 285–290. [[CrossRef](#)]
36. Yin, H.; Zhou, Y.; Ma, Q.; Ai, S.; Chen, Q.; Zhu, L. Electrocatalytic oxidation behavior of guanosine at graphene, chitosan and Fe₃O₄ nanoparticles modified glassy carbon electrode and its determination. *Talanta* **2010**, *82*, 1193–1199. [[CrossRef](#)]
37. Teymourian, H.; Salimi, A.; Khezrian, S. Fe₃O₄ magnetic nanoparticles/reduced graphene oxide nanosheets as a novel electrochemical and bioelectrochemical sensing platform. *Biosens. Bioelectron.* **2013**, *49*, 1–8. [[CrossRef](#)]
38. Sun, Y.; Zhang, W.; Yu, H.; Hou, C.; Li, D.; Zhang, Y.; Liu, Y. Controlled synthesis various shapes Fe₃O₄ decorated reduced graphene oxide applied in the electrochemical detection. *J. Alloy Compd.* **2015**, *638*, 182–187. [[CrossRef](#)]
39. He, Q.; Lang, J.; Li, G.; Deng, P.; Liu, J.; Liu, X. Electrochemical Detection of Dopamine Based on MnO₂ Nanowires/Reduced Graphene Oxide Composites Modified Glassy Carbon Electrode. *Chin. J. Anal. Chem.* **2018**, *46*, 438–445.
40. Wu, D.; Li, Y.; Zhang, Y.; Wang, P.; Wei, Q.; Du, B. Sensitive electrochemical sensor for simultaneous determination of dopamine, ascorbic Acid, and uric acid enhanced by amino-group functionalized mesoporous Fe₃O₄@graphene sheets. *Electrochim. Acta* **2014**, *116*, 244–249. [[CrossRef](#)]
41. Guo, S.; Li, D.; Zhang, L.; Li, J.; Wang, E. Monodisperse mesoporous superparamagnetic single-crystal magnetite nanoparticles for drug delivery. *Biomaterials* **2009**, *30*, 1881–1889. [[CrossRef](#)] [[PubMed](#)]
42. Yang, S.; Wang, G.; Li, G.; Du, J.; Qu, L. Decoration of graphene modified carbon paste electrode with flower-globular terbium hexacyanoferrate for nanomolar detection of rutin. *Electrochim. Acta* **2014**, *144*, 268–274. [[CrossRef](#)]
43. Bard, A.J.; Faulkner, L.R. *Electrochemical Methods: Fundamentals Applications*, 2nd ed.; Wiley: New York, NY, USA, 2001.
44. Guo, H.L.; Wang, X.F.; Qian, Q.Y.; Wang, F.B.; Xia, X.H. A green approach to the synthesis of graphene nanosheets. *ACS Nano* **2009**, *3*, 2653–2659. [[CrossRef](#)] [[PubMed](#)]
45. Xiong, H.; Jin, B. The electrochemical behavior of AA and DA on graphene oxide modified electrodes containing various content of oxygen functional groups. *J. Electroanal. Chem.* **2011**, *661*, 77–83. [[CrossRef](#)]



© 2019 by the authors. Licensee MDPI, Basel, Switzerland. This article is an open access article distributed under the terms and conditions of the Creative Commons Attribution (CC BY) license (<http://creativecommons.org/licenses/by/4.0/>).